Original Research Article: full paper

(2023), «EUREKA: Physics and Engineering»
Number 2

NUMERICAL COMPARISON AND EFFICIENCY ANALYSIS OF THREE VERTICAL AXIS TURBINE OF H-DARRIEUS TYPE

Angie Guevara-Munoz ✉
Department of Mechatronics Engineering[1]
angieguevara220191@correo.itm.edu.co

Diego Hincapie-Zuluaga
Department of Mechatronics Engineering[1]

Jorge Sierra-Del Rio
Department of Mechanical Engineering[1]

Miguel Angel Rodriguez-Cabal
Department of Mechatronics Engineering[1]

Edwar Torres-Lopez
Department of Mechanical Engineering
Research Group – GEA
Universidad de Antioquia
Cl. 67 #53-108, Medellín, Antioquia, Colombia, 050010

[1]*Research Group – MATyER*
Instituto Tecnológico Metropolitano
Cl. 75 #75-101, Medellín, Antioquia, Colombia, 050036

✉**Corresponding Author**

Abstract

Hydropower is an important source of energy in Latin America. Many countries in the region, including Brazil, Peru, Colombia, and Chile, rely heavily on hydropower plants to meet their energy needs. However, there are also challenges related to the use of hydropower in the region, such as the construction of dams that can have negative impacts on ecosystems and local communities. A new alternative is the production of energy through hydrokinetic turbines because they are a clean and renewable energy source that does not emit greenhouse gases. In addition, its production is predictable and can be generated in a variety of environments, from coasts to rivers and canals. Within the hydrokinetic turbines are the H-Darrieus turbines although they are still under development, they are seen as an important opportunity to diversify the energy matrix and reduce dependence on fossil fuels. The main purpose of this study is to determine and compare the efficiency of three Darrieus H-type vertical axis hydrokinetic turbines numerically. The turbines were configured with different solidities. The NACA 0018 profile was used for the turbine design. The study was carried out using the ANSYS® Fluent 2022R2 software, two-dimensional (2D) simulations set up constant operating conditions. Rotation speed variations have been set between 21 and 74 RPM with 10 rpm increments. Furthermore, the General Richardson extrapolation method is used for the analysis of mesh convergence, monitoring the turbine power coefficient as a convergence parameter. The numerical results show that the turbine H-Darrieus with a solidity of 1.0, a wider operating range, and lower power and torque coefficient. At low TRS, the largest solidity provided the best efficiency and the greatest self-starting capability, but it also had the smallest operating range.

Keywords: CFD, Hydrokinetic turbine, H-Darrieus, Ansys Fluent, TSR, Efficiency, Solidity, General Richardson extrapolation, NACA 0018.

DOI: 10.21303/2461-4262.2023.002593

1. Introduction

Hydrokinetic Turbines (HTs) operate under the same operating principle as wind turbines [1, 2], but take advantage of the natural flow of water to produce electricity. HTs are considered a viable option with low environmental impact [3] because they operate, at zero head conditions (0 meters), they do not require dams or storage ponds, they are easy to maintain [4] and their

operation is uninterrupted (if water flows continuously). HTs can be installed in the ocean, rivers, or artificial canals, and they can be classified into two types according to the position of their axis: axial flow turbines, whose axis of rotation follows the direction of flow, and crossflow turbines, whose axis of rotation is located perpendicular to the direction of flow. Crossflow HTs are the most used H-Darrieus Turbines (HDTs), which can be considered a viable option for hydrogenation [5, 6]. In recent years, there has been a considerable increase in interest in this technology, where research has focused on improving the power coefficient C_p and torque to increase its efficiency. Different types of research have been carried out, these can be divided into 3 main fields, numerical, experimental, numerical-experimental. The numerical studies evaluate by means of Computational Fluid Dynamics (CFD) the hydraulic behavior of the HDTs, generally the simulations are performed in transient state and are mostly configured with the SST k-ω (Shear Stress Transport k-ω) or k-e Realizable turbulence models, because they correctly predict the turbine behavior, and their computational cost is acceptable [7–11].

HDTs are mainly composed of three main components (**Fig. 1**), the central shaft, which transmits the kinetic energy extracted from the fluid to an electric generator, and the support arms that support a series of blades that are driven by interacting with the fluid, this occurs due to the geometric characteristics of the blades that are located on the periphery [12]. The blade geometry constitutes a fundamental part for the good performance of the turbine, due to the pressure forces that are developed when it is subjected to an incident flow. The lift forces on each blade contribute to the total rotor torque, which is then transferred to the generator through the main shaft and other drive train components [13]. Also, the number of blades is a fundamental parameter because it is directly related to the solidity [13], it also has a great impact on the overall dynamic behavior of the HDTs [14]. The solidity is a fundamental parameter that determines the geometry of the HDTs and has a significant influence on the HDTs behavior [15]. Symmetric profiles are the most used for wind turbines such as the NACA symmetric profiles with 4 digits (0012, 0015, and 0018) [16, 17], especially the NACA0018 profile.

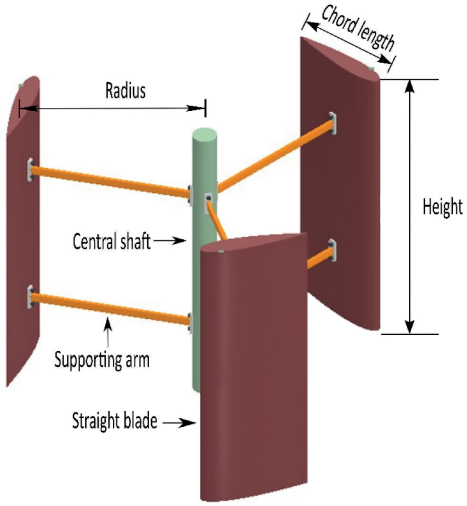

Fig. 1. Components of the H-Darrieus rotor. Own source

This study aims to evaluate and compare the performance of three H-Darrieus hydrokinetic turbines of symmetrical profile type NACA 0018 numerically. The rest of the paper is divided in three parts: first, describes the operative principles of the turbine and the research procedure. Second, the results of the torque coefficient and power coefficient of the turbines are analyzed and discussed, and the last section are the conclusions of the research.

2. Materials and methods

Turbine modeling: in this work, three H-Darrieus turbines with low solidities were designed to analyze their performance by means of Computational Fluid Dynamics (CFD) method. The commercial package ANSYS FLUENT® 2022R2 was used to conduct this study. In addition, the General Richardson extrapolation method was implemented to perform the mesh sensitivity analysis.

2. 1. Mathematic model

Usually, the most important parameters in H-Darrieus turbine investigations are the power coefficient C_p and the torque coefficient C_T because they relate the mechanical power output P_T and the torque of force T on the turbine shaft:

$$C_p = \frac{P_T}{0.5\rho A U^3}, \tag{1}$$

$$C_t = \frac{T}{0.5 A U^2}. \tag{2}$$

Where, ρ is the density, A is the projected area of the rotor and U is the water velocity. Additionally, solidity σ is an important parameter of HDTs since it can strongly influence the performance of the turbine [18], because this parameter compares the number of blades N and their chord length c with respect to the turbine rotation radius R, this can be calculated by:

$$\sigma = \frac{N_c}{R}. \tag{3}$$

On the other hand, there is another dimensionless parameter that has a great influence on the efficiency of the [19, 20] turbine. The TSR λ (Tip Speed Ratio) indicates the speed of the blade at its tip and the current velocity. Where, ω is the angular velocity:

$$\lambda = \frac{\omega R}{U}. \tag{4}$$

2. 2. Turbine design

The H-Darrieus turbine profile used in this study are shown in **Fig. 2**, it is symmetrical NACA 0018 profile. It was configured with different chord length to vary the solidity.

The designed turbines have 3 blades and a constant rotation radius, its solidities are 1.0, 1.35, and 1.79 respectively. The design is done in 2D in the SpaceClaim module of Ansys® 2022, the dimensions are shown **Fig. 3**, each part of the rotor is designed individually to implement the mesh overlapping method in Ansys Fluent® 2022.

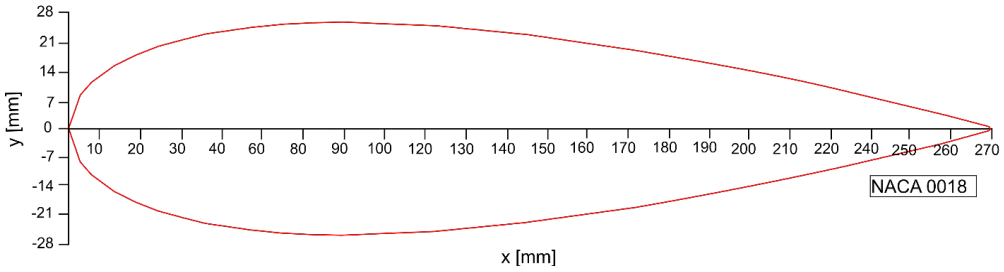

Fig. 2. NACA 0018 profile. Own source

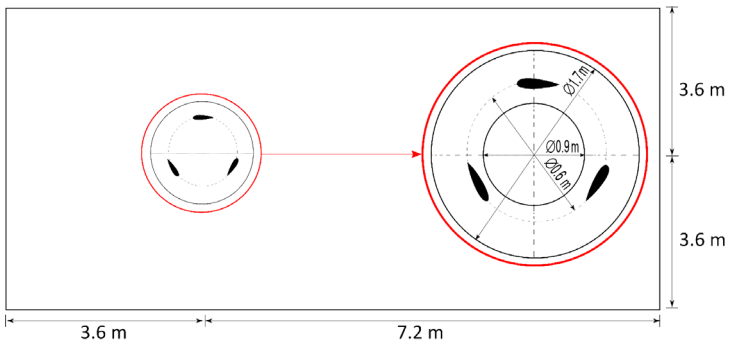

Fig. 3. Channel and rotor dimensions. Own source

2. 3. Grid generation and boundary conditions

ICEM CFD module from ANSYS® R2022 is used for the grid generation of the complete domain. The structured grid is generated for each domain. Rectangular elements were used to represent the internal surface of each of the HDT components. **Fig. 4, *a*** shows stationary and rotary domain that corresponds to the water channel and the rotor. **Fig. 4**, ***b, c*** shows the rotor mesh and the blade discretization. It is possible to identify the inflation performed on the blade walls, with a growth rate of 1.2.

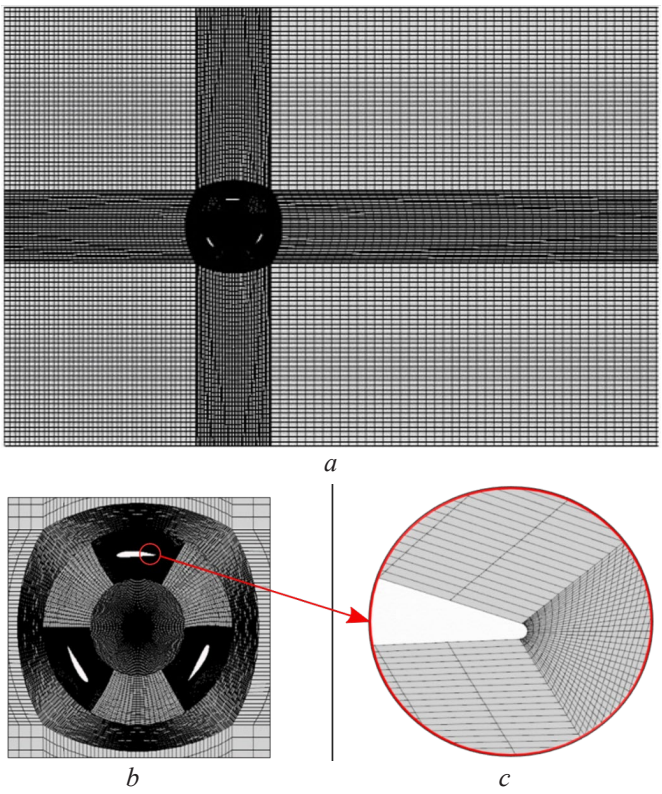

Fig. 4. Discretization of control surfaces. Own source: *a* – Channel grid mesh; *b* – Rotor mesh; *c* – Blade mesh

A grid convergence analysis was carried out using the General Richardson extrapolation method. The control variable selected as the convergence parameter is power coefficient. The turbine with solidity of 1.79 configured with a TSR of 1.5 was selected to carry out the independence study. Based on the General Richardson extrapolation method, the exact solution can be calculated based on mesh convergence and mesh refining [21, 22]. To apply the General Richardson extrapolation, the convergence ratio needs to be calculated with the following equation [23, 24]:

$$R^* = \frac{\phi_2 - \phi_1}{\phi_3 - \phi_2}. \quad (5)$$

Where ϕ_1, ϕ_2 and ϕ_3 is the solution (convergence parameter, in this case the power coefficient) of the finest, median, and coarsest mesh. According to the R^* value, the following conditions are applicable:

$R^* > 1$: Monotonic divergence;

$1 > R^* > 0$: Monotonic convergence;

$0 > R^* > -1$: Oscillating convergence;

$R^* < -1$: Oscillating divergence.

General Richardson extrapolation can only be used if the convergence condition is monotonic. The General Richardson extrapolation can be calculated as follows:

$$VR = \phi_1 + \frac{\phi_1 - \phi_2}{r_r - 1}. \quad (6)$$

Where r is the refinement ratio between fine and coarse mesh size, defined as $r = \left(\frac{N^{\circ} fine}{N^{\circ} coarse}\right)^{0.5}$ and p is the global convergence order of the solution, corresponding to $\rho = \frac{\ln(R^*)}{\ln(r)}$.

2.4. Numeric solution

The simulation is conducted in transitory state in the commercial program Fluent of ANSYS® 2022. A velocity inlet of 1 m/s at the inlet, at atmospheric pressure outlet was stablished for the outlet opening. Interfaces are shared by sliding meshes configuration. In addition, for the rotating domain, an angular velocity was established from 21 to 74 rpm. The boundary conditions established for the static and rotating domains are shown in **Fig. 5**.

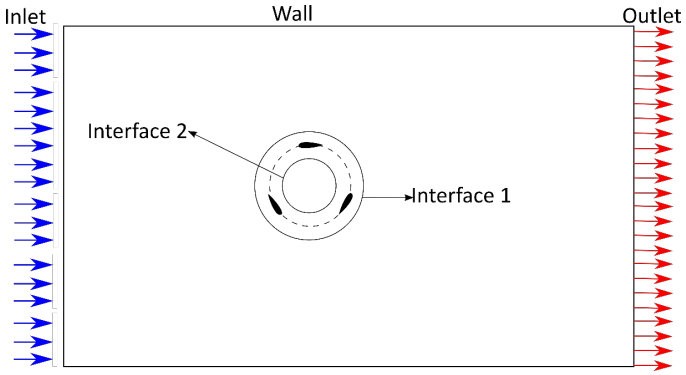

Fig. 5. Boundary conditions for the control surfaces. Own source

The equations of government are the continuity and Reynolds Averaged Navier-Stokes equations (URANS), which are formulations of the laws of conservation of mass, torque, and energy, these are written as follows [25, 26]:

$$\frac{\partial U_i}{\partial t} + \frac{\partial U_i}{\partial x_j} = 0, \quad (7)$$

$$\frac{\partial U_i}{\partial t} + U_i \frac{\partial U_i}{\partial x_j} = -\frac{1}{\rho}\frac{\partial P}{\partial x_i} + \frac{\partial}{\partial x_j}\left[v\left(\frac{\partial U_i}{\partial x_j} + \frac{\partial U_j}{\partial x_i} - \frac{2}{3}\delta_{ij}\frac{\partial U_i}{\partial x_i}\right) + \frac{\partial}{\partial x_j}\left(-\overline{u_i' u_j'}\right)\right]. \quad (8)$$

In the present study, the *k-e* Realizable turbulence model was used because they correctly predict turbine behavior, and their computational cost is accepTable in comparison with other turbulence models available in the solver [7–11]. The transport equations for k and ε in this turbulence model are given by the following [27]:

$$\frac{\partial}{\partial t}(\rho k) + \frac{\partial}{\partial x_i}(\rho k U_j) = \frac{\partial}{\partial x_i}\left[\left(\mu + \frac{\mu_t}{\sigma_k}\right)\frac{\partial k}{\partial x_j}\right] + G_k + G_b - \rho\varepsilon - Y_M + S_k, \quad (9)$$

$$\frac{\partial}{\partial t}(\rho\varepsilon) + \frac{\partial}{\partial x_j}(\rho\varepsilon U_j) = \frac{\partial}{\partial x_j}\left[\left(\mu + \frac{\mu_t}{\sigma_\varepsilon}\right)\frac{\partial \varepsilon}{\partial x_j}\right] + \rho C_1 S_t - \rho C_2 \frac{\varepsilon^2}{k + \sqrt{v\varepsilon}} + C_{1\varepsilon}\frac{\varepsilon^2}{\kappa} C_{3\varepsilon} G_b + S_t. \quad (10)$$

Where:

$$C_1 = max\left[0.43\frac{\eta}{\eta + 5}\right], \quad (11)$$

$$\eta = S\frac{k}{\varepsilon}, \quad (12)$$

$$S = \sqrt{2S_{ij}S_{ij}}. \quad (13)$$

Where G_k is the generation of turbulence kinetic energy caused by velocity gradients, G_b is the generation of turbulence kinetic energy due to buoyancy, Y_M is the contribution of fluctuating diffusion in compressible turbulence to the overall dissipation rate, σ_k and σ_e are the turbulent Prandtl numbers for k and e, respectively, S_k and S_e are user-defined source terms.

3. Results and discussion

3. 1. Mesh convergence study

In this paper, the analysis of the mesh convergence was carried out using three meshes *M*1 (fine mesh), *M*2 (medium mesh) and *M*3 (coarse mesh). The data obtained by means of the General Richardson extrapolation method are shown in **Table 1**.

Table 1
Summary of mesh convergence using General Richardson extrapolation. Own source

Number of cells (X10^5)	Power coefficient [–]	R*[–]	*r* [–]	*p* [–]	Richardson value [–]	Relative error [%]
1.02 (M3)	0.474					–0.122
1.33 (M2)	0.427	0.087	1.22	12.33	0.422	–0.011
1.53 (M1)	0.423					0.001

Fig. 6 depicts the mesh independence study conducted. Considering that the power coefficient value with the extrapolation is 0.422, the selected mesh is the *M*2 because it presents an error of 0.01 % and offers lower computational cost.

The metrics of the realized meshes are illustrated in **Table 2** which are in the acceptable ranges as suggested by ANSYS user manuals, such as minimum quality (greater than 0.3), maximum aspect ratio (less than 100) [28] and minimum 2×2×2 determinant (greater than 0.3) [29].

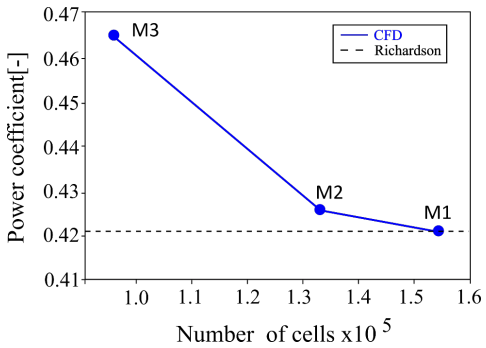

Fig. 6. Mesh independence study. Own source

Table 2
Mesh details and metrics. Own source

Components	Number of elements	Min. Determinant 2×2×2	Max. Aspect ratio
Rotor solidity of 1.0	15484	0.310	91.00
Rotor solidity of 1.35	16558	0.485	96.00
Rotor solidity of 1.79	17354	0.595	98.00
Channel	117521	0.648	5.07

3. 2. Influence of solidity on hydraulic behavior

By analyzing the pressure and velocity fields for the last revolution of the solidity 1.0, 1.35, and 1.79 cases, it is possible to qualitatively determine if the simulations correctly emulate the hydraulic behavior of the HDTs. Additionally, it is possible to observe if the critical points that are

located on the blade walls are capturing the velocities and pressures that develop there, corroborating the excellent quality of the meshes. **Fig. 7, *a–c***, show the pressure contours of solidity of 1.0, 1.35, and 1.79 cases respectively. In **Fig. 7** it is possible to observe the general pressure contour in the rotating domain. In all cases, the lowest pressures are generated inside the rotor. **Fig. 7** also shows the pressure contour in blade 1 (first blade from left to right). It is evident that the higher the solidity, the more significant the increase and pressure drop experienced by the walls of the blades.

Likewise, **Fig. 8** shows the blade velocity contour reported in solidity of 1.0, 1.35, and 1.79, respectively. It is possible to observe that in that the blade meshes and the implemented turbulence model captured the physical phenomena in the viscous layer of the blade walls.

The increase in solidity directly affects the behavior of the HDTs. In **Fig. 9**, the velocity current lines are observed in the cases solidity of 1.0, 1.35, and 1.79 respectively. It is shown that the front part of the rotor exhibits laminar behavior, while the stream downstream of the rotor is more turbulent. The wake is more intense in the case of solidity of 1.79 because it has a greater solidity, this behavior coincides with that reported in the literature [18].

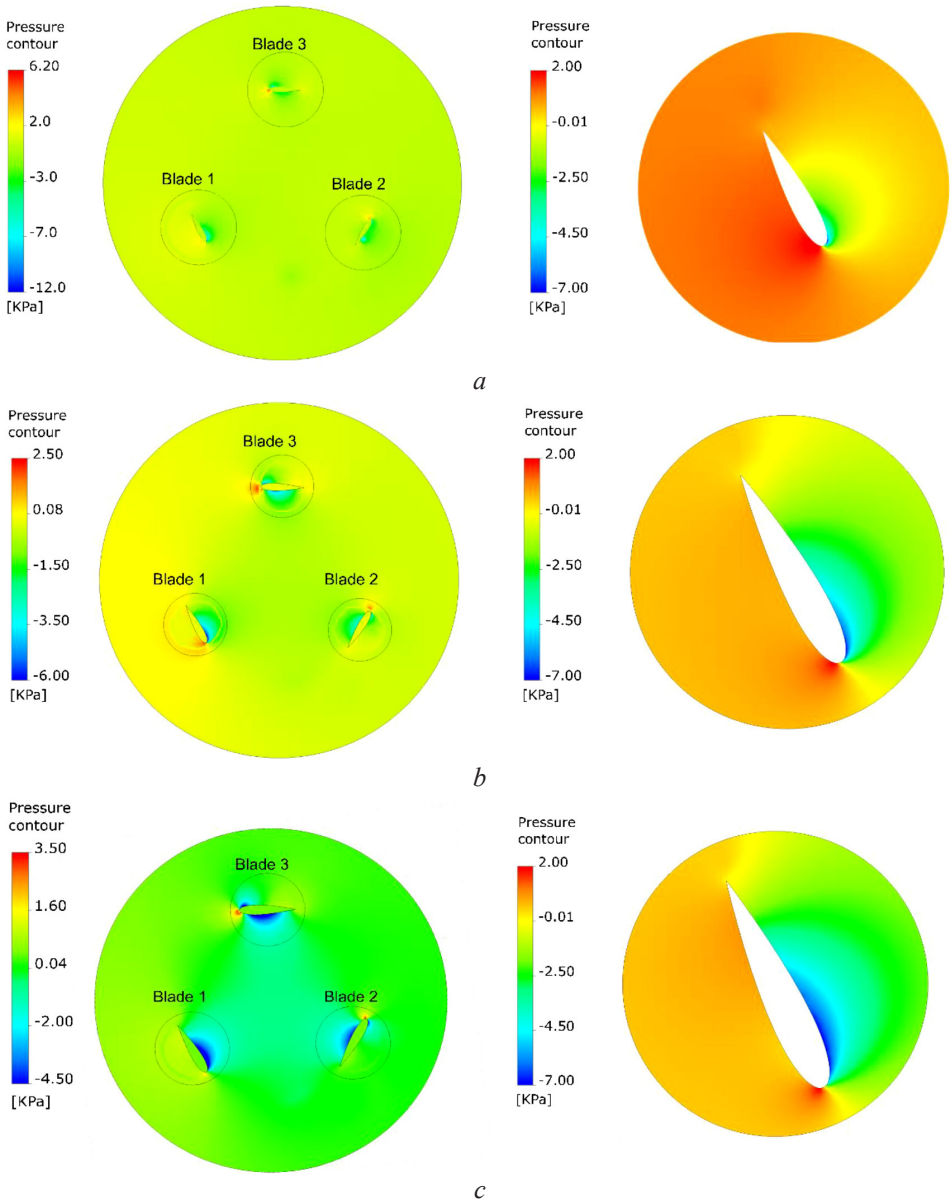

Fig. 7. Pressure contours of the rotating domains: *a* – Solidity of 1.0; *b* – Solidity of 1.35; *c* – Solidity of 1.79. Own source

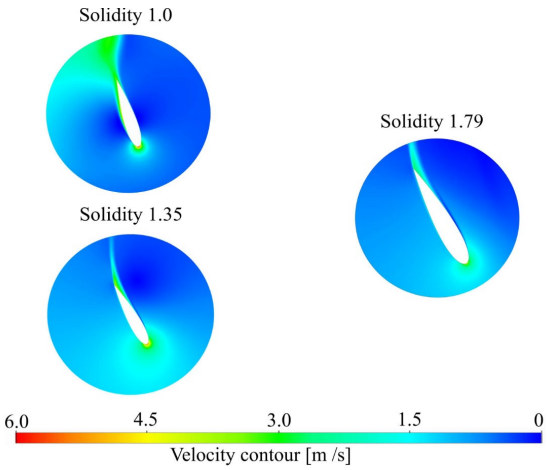

Fig. 8. Blade velocity contours. Own source

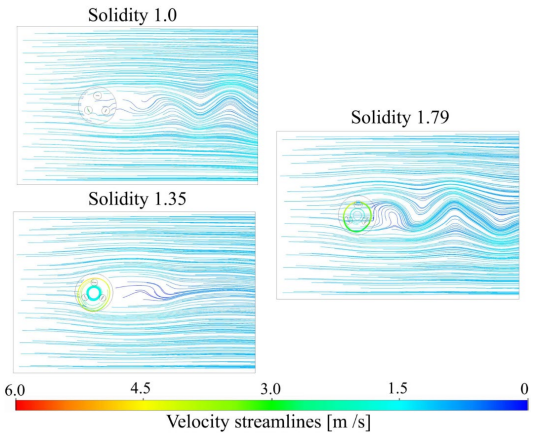

Fig. 9. Velocity streamlines. Own source

The behavior of the power coefficient C_p of the HDTs when varying the TSR normally has a parabolic behavior, which means that there is a range of the TSR where the maximum efficiency is reached. According to [30] by increasing the solidity the maximum C_p is obtained at lower TSR. This behavior is illustrated in **Fig. 10**, where the C_p versus TSR of the cases is observed.

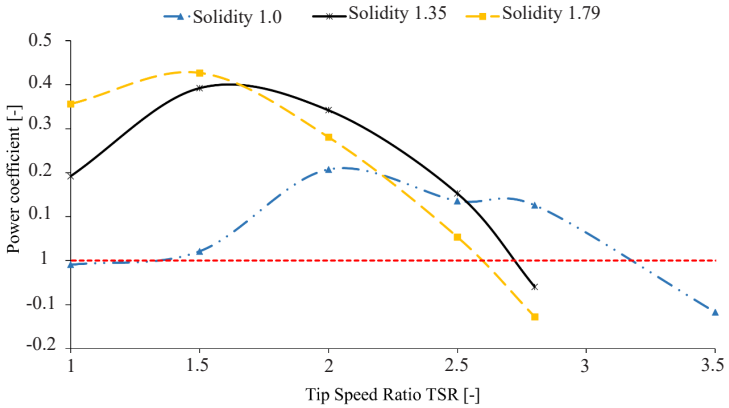

Fig. 10. Performance at different TSR. Own source

3. 3. Effect of solidity on torque coefficient

The cyclic and harmonic behavior of the C_t is typical in H-Darrieus hydrokinetic turbines, this movement can oscillate between the positive and negative *Y*-axis if the movement predomi-

nates in the negative *Y*-axis zone. It is indicating that the turbine is not operating in those ranges, it is inefficient. **Fig. 11, *a*–c** shows the variation of the total C_t over the last revolution for each of the solidity of 1.0, 1.35, and 1.79 respectively. It is possible to identify a red dotted line that indicates zero, thus marking when the C_t is positive or negative.

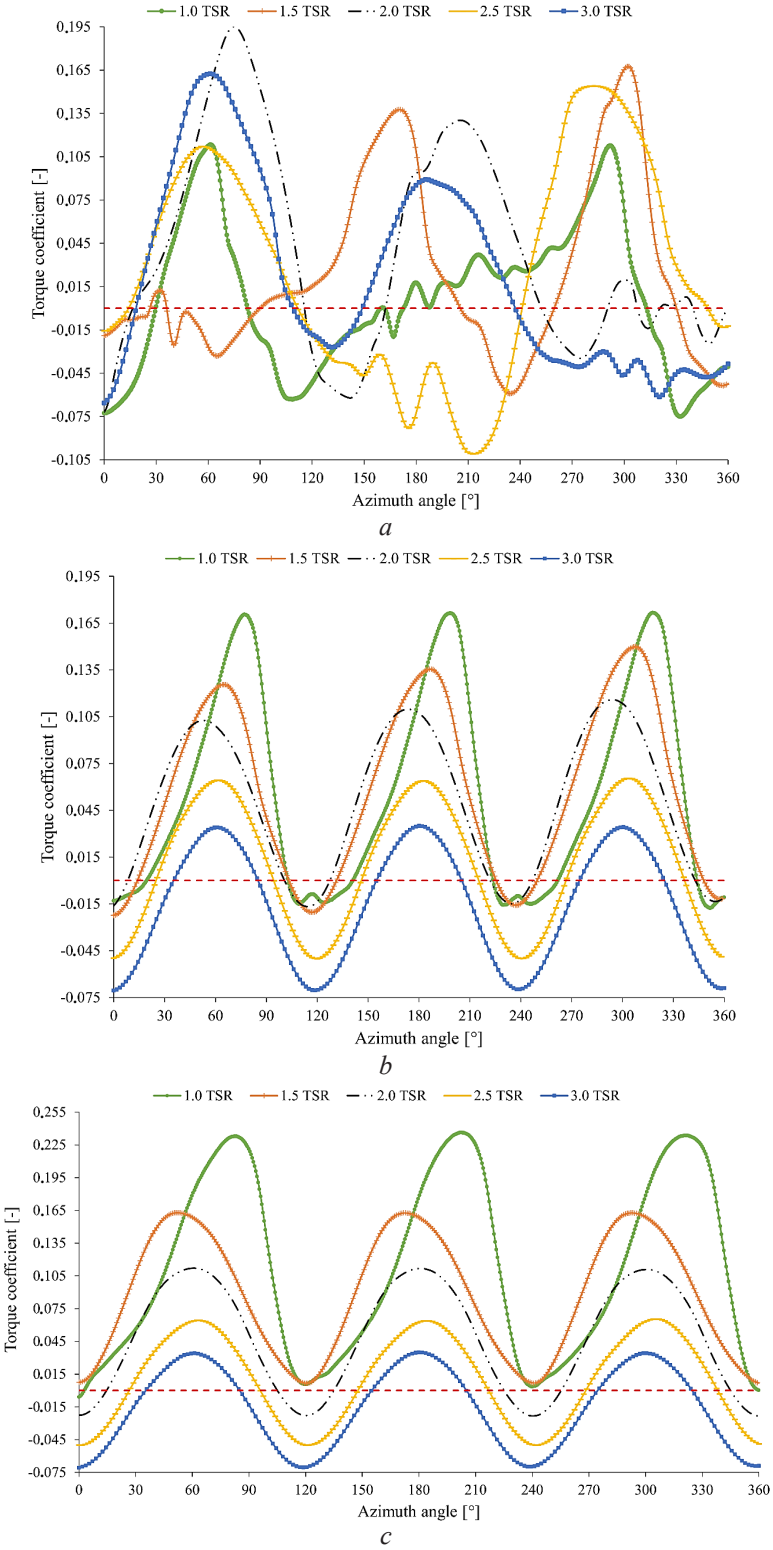

Fig. 11. Variation of total C_t in the last revolution: *a* – solidity 1.0; *b* – solidity 1.35; *c* – solidity 1.79. Own source

The average torque coefficients for each case were analyzed, and it was found that the best self-starting turbine has the turbine with solidity of 1.79 with 1.0 TSR, as it has the highest positive net torque. **Table 3** shows the results obtained numerically for each of the best cases for each solidity. It is observed that, although solidity obtained the best torque coefficient, it does not have the highest efficiency, and this is because its performance is better than 1.5 TSR. **Fig. 12** shows the behavior of the best cases for each solidity in one turn. The turbine with a solidity of 1.79 has the highest and lowest peaks compared to the other cases. The turbine with a solidity of 1.35 exhibits sTable behavior. In contrast, the turbine with a solidity of 1.0 has an irregular torque coefficient and is the most negative of all cases.

Table 3

Summary of maximums C_t. Own source

Solidity	TSR	Torque coefficient [–]	Average torque [Nm]	Power [Watt]	Power coefficient [–]	Efficiency [%]
1.0	2.0	0.09	20.933	93.036	0.207	20.737
1.35	1.5	0.07	52.823	176.080	0.392	39.247
1.79	1.0	0.12	71.931	159.847	0.356	35.628

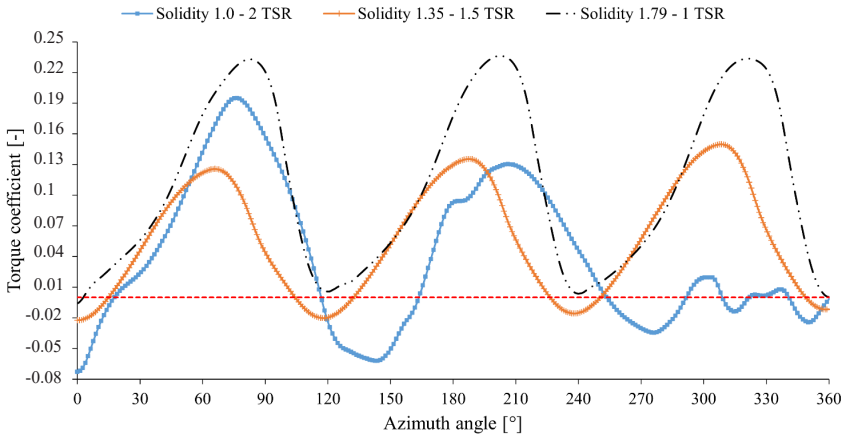

Fig. 12. Variation of total C_t. Own source

3. 4. Research limitations and directions of developed

Modeling is a valuable tool for the design and optimization of hydrokinetic turbines such as the H-Darrieus turbines. However, the complexity of the flows surrounding these turbines can make a simulation costly in terms of time and computational resources. One way to simplify modeling is using simplified models. In this sense, a simplified model of H-Darrieus turbine is a mathematical and simplified representation of the turbine in which certain complex flow characteristics are omitted. This type of model allows simulations to be carried out in a much shorter time than more complex models, which makes them very useful for the design and optimization of hydrokinetic turbines.

However, by simplifying the model, certain important flow characteristics that can affect turbine efficiency may be lost. Therefore, it is important to know the limitations of simplified models and their ability to adequately represent the flow characteristics in the hydrokinetic turbine. Accordingly, this paper explores the limitations of a simplified model of H-Darrieus turbine eliminating the central drive shaft and support arms using CFD in two dimensions (2D) (**Fig. 1** and **Fig. 3**).

Therefore, it is important in future work to consider the complete design of the H-Darrieus turbine in three dimensions to obtain more realistic results in certain flow characteristics, such as turbulence and vortices. In addition, fluid-structure interactions, which may be important in the design and efficiency evaluation of the H-Darrieus turbines evaluated in this study.

On the other hand, it is important to consider experimental validation when evaluating the accuracy of the simulation models used. However, prior to this step, studies could be conducted to evaluate the design materials and structures, since this is also a critical factor in the performance and durability of hydrokinetic turbines. Prolonged exposure to water currents and flow impacts can cause wear and

damage to turbine materials and structures. Therefore, careful evaluation of the materials and structures used in the construction of hydrokinetic turbines is essential to ensure their long-term performance.

As such, fatigue analysis techniques, strength tests and impact simulations can be used to assess the performance and durability of turbine materials and structures. Optimization of turbine materials and structures can significantly improve turbine performance and service life, which can contribute to the adoption and success of hydrokinetic energy.

4. Conclusions

Using computational tools, a numerical study was performed in ANSYS® R2022, the torque coefficient and power coefficient were evaluated of H-Darrieus rotors of symmetric profile type NACA 0018 configured with solidities of 1.0, 1.35, and 1.79. The results showed that increase in solidity is equivalent to a decrease in the tip speed ranges and an increase in the maximum rotor power.

Larger solidities exhibit higher cyclic stability and higher torque coefficient. The turbine with a solidity of 1.79 performed better compared to the solidity of 1.35. However, the self-starting capability is higher in the 1.35 rotor, making it a more viable option for implementation. Since this study does not consider three-dimensional effects, future work is expected to include 3D simulation. Furthermore, proceed with the experimental validation of the different models proposed.

Conflict of interest

The authors declare that they have no conflict of interest in relation to this research, whether financial, personal, authorship or otherwise, that could affect the research and its results presented in this paper.

Financing

This research was funded by Instituto Tecnológico Metropolitano (ITM) through Project P20217 ascribed to the Call for the creation of a bank of eligible projects CTIC from ITM.

Data availability

Data cannot be made available for reasons disclosed in the data availability statement.

Acknowledgements

The authors gratefully acknowledge the Instituto Tecnológico Metropolitano and its Research Group on Advanced Materials and Energy (MATyER) for the use of equipment and spaces necessary to conduct this research.

References

[1] Khan, M. J., Bhuyan, G., Iqbal, M. T., Quaicoe, J. E. (2009). Hydrokinetic energy conversion systems and assessment of horizontal and vertical axis turbines for river and tidal applications: A technology status review. Applied Energy, 86 (10), 1823–1835. doi: https://doi.org/10.1016/j.apenergy.2009.02.017

[2] Anyi, M., Kirke, B. (2015). Tests on a non-clogging hydrokinetic turbine. Energy for Sustainable Development, 25, 50–55. doi: https://doi.org/10.1016/j.esd.2015.01.001

[3] Yuce, M. I., Muratoglu, A. (2015). Hydrokinetic energy conversion systems: A technology status review. Renewable and Sustainable Energy Reviews, 43, 72–82. doi: https://doi.org/10.1016/j.rser.2014.10.037

[4] Furukawa, A., Watanabe, S., Matsushita, D., Okuma, K. (2010). Development of ducted Darrieus turbine for low head hydropower utilization. Current Applied Physics, 10 (2), S128–S132. doi: https://doi.org/10.1016/j.cap.2009.11.005

[5] Khan, M. J., Iqbal, M. T., Quaicoe, J. E. (2008). River current energy conversion systems: Progress, prospects and challenges. Renewable and Sustainable Energy Reviews, 12 (8), 2177–2193. doi: https://doi.org/10.1016/j.rser.2007.04.016

[6] Sornes, K. (2010). Small-scale Water Current Turbines for River Applications. ZERO. Available at: https://zero.no/wp-content/uploads/2016/05/small-scale-water-current-turbines-for-river-applications.pdf

[7] Wang, S., Ingham, D. B., Ma, L., Pourkashanian, M., Tao, Z. (2012). Turbulence modeling of deep dynamic stall at relatively low Reynolds number. Journal of Fluids and Structures, 33, 191–209. doi: https://doi.org/10.1016/j.jfluidstructs.2012.04.011

[8] Almohammadi, K. M., Ingham, D. B., Ma, L., Pourkashan, M. (2013). Computational fluid dynamics (CFD) mesh independency techniques for a straight blade vertical axis wind turbine. Energy, 58, 483–493. doi: https://doi.org/10.1016/j.energy.2013.06.012

[9] Lanzafame, R., Mauro, S., Messina, M. (2014). 2D CFD Modeling of H-Darrieus Wind Turbines Using a Transition Turbulence Model. Energy Procedia, 45, 131–140. doi: https://doi.org/10.1016/j.egypro.2014.01.015

[10] Daróczy, L., Janiga, G., Petrasch, K., Webner, M., Thévenin, D. (2015). Comparative analysis of turbulence models for the aerodynamic simulation of H-Darrieus rotors. Energy, 90, 680–690. doi: https://doi.org/10.1016/j.energy.2015.07.102

[11] Marsh, P., Ranmuthugala, D., Penesis, I., Thomas, G. (2017). The influence of turbulence model and two and three-dimensional domain selection on the simulated performance characteristics of vertical axis tidal turbines. Renewable Energy, 105, 106–116. doi: https://doi.org/10.1016/j.renene.2016.11.063

[12] Çetin, N., Yurdusev, M., Ata, R., Özdamar, A. (2005). Assessment of Optimum Tip Speed Ratio of Wind Turbines. Mathematical and Computational Applications, 10 (1), 147–154. doi: https://doi.org/10.3390/mca10010147

[13] Mon, E. E. (2019). Design of Low Head Hydrokinetic Turbine. International Journal of Trend in Scientific Research and Development, 3 (5).

[14] Bel Mabrouk, I., El Hami, A. (2019). Effect of number of blades on the dynamic behavior of a Darrieus turbine geared transmission system. Mechanical Systems and Signal Processing, 121, 562–578. doi: https://doi.org/10.1016/j.ymssp.2018.11.048

[15] Tobon-Tobon, N., Henao-González, K. A., Burbano-Hernandez, A. F., Sierra-Del Rio, J., Hincapié Zuluaga, D. A. (2020). Influencia de la solidez y el número de álabes en una turbina de eje vertical tipo H-darrieus. Revista Politécnica, 16 (32), 9–18. doi: https://doi.org/10.33571/rpolitec.v16n32a1

[16] Kumar, A., Saini, R. P. (2017). Techno-Economic Analysis of Hydrokinetic Turbines. doi: https://doi.org/10.20944/preprints201704.0072.v1

[17] Alam, Md. J., Iqbal, M. T. (2009). Design and development of hybrid vertical axis turbine. 2009 Canadian Conference on Electrical and Computer Engineering. doi: https://doi.org/10.1109/ccece.2009.5090311

[18] Qamar, S. B., Janajreh, I. (2017). A comprehensive analysis of solidity for cambered darrieus VAWTs. International Journal of Hydrogen Energy, 42 (30), 19420–19431. doi: https://doi.org/10.1016/j.ijhydene.2017.06.041

[19] Anyi, M., Kirke, B. (2011). Hydrokinetic turbine blades: Design and local construction techniques for remote communities. Energy for Sustainable Development, 15 (3), 223–230. doi: https://doi.org/10.1016/j.esd.2011.06.003

[20] Roy, S., Saha, U. K. (2015). Wind tunnel experiments of a newly developed two-bladed Savonius-style wind turbine. Applied Energy, 137, 117–125. doi: https://doi.org/10.1016/j.apenergy.2014.10.022

[21] Roache, P. J. (1994). Perspective: A Method for Uniform Reporting of Grid Refinement Studies. Journal of Fluids Engineering, 116 (3), 405–413. doi: https://doi.org/10.1115/1.2910291

[22] Eça, L., Hoekstra, M. (2006). Discretization Uncertainty Estimation based on a Least Squares version of the Grid Convergence Index. 2nd Workshop on CFD Uncertainty Analysis. Lisbon.

[23] Roache, P. J. (1997). Quantification of uncertainty in computational fluid dynamics. Annual Review of Fluid Mechanics, 29 (1), 123–160. doi: https://doi.org/10.1146/annurev.fluid.29.1.123

[24] Roache, P. J. (2003). Conservatism of the Grid Convergence Index in Finite Volume Computations on Steady-State Fluid Flow and Heat Transfer. Journal of Fluids Engineering, 125 (4), 731–732. doi: https://doi.org/10.1115/1.1588692

[25] Hashem, I., Mohamed, M. H. (2018). Aerodynamic performance enhancements of H-rotor Darrieus wind turbine. Energy, 142, 531–545. doi: https://doi.org/10.1016/j.energy.2017.10.036

[26] Mohamed, M. H., Dessoky, A., Alqurashi, F. (2019). Blade shape effect on the behavior of the H-rotor Darrieus wind turbine: Performance investigation and force analysis. Energy, 179, 1217–1234. doi: https://doi.org/10.1016/j.energy.2019.05.069

[27] Mohamed, M. H., Ali, A. M., Hafiz, A. A. (2015). CFD analysis for H-rotor Darrieus turbine as a low speed wind energy converter. Engineering Science and Technology, an International Journal, 18 (1), 1–13. doi: https://doi.org/10.1016/j.jestch.2014.08.002

[28] CFX Solver Modelling Guide, Release 15.0 (2013). ANSYS CFX–Solver Modeling Guide. Ansys Inc., 15317, 724–746.

[29] User Manual Ansys ICEM CFD 12.1 (2009). Ansys Inc., 0844682, 724–746.

[30] Mohamed, M. H. (2013). Impacts of solidity and hybrid system in small wind turbines performance. Energy, 57, 495–504. doi: https://doi.org/10.1016/j.energy.2013.06.004

Received date 31.12.2022
Accepted date 28.02.2023
Published date 22.03.2023

How to cite: *Guevara-Munoz, A., Hincapie-Zuluaga, D., Sierra-Del Rio, J., Rodriguez-Cabal, M. A., Torres-Lopez, E. (2023). Numerical comparison and efficiency analysis of three vertical axis turbine of H-Darrieus type. EUREKA: Physics and Engineering, 2, 28–39. doi: https://doi.org/10.21303/2461-4262.2023.002593*